Kovove Mater. 62 2024 295–301
DOI: 10.31577/km.2024.5.295

Effect of cold rolling reduction rate on high-temperature plasticity of 3207 duplex stainless steel

Jing Wang[1], Rui Fu[1], Lei Ba[1]*, Jingkun Li[2]**

[1] *Ordos Vocational College, Ordos 017000, P. R. China*
[2] *Hebei Key Laboratory of New Functional Materials, School of Material Science and Engineering, Hebei University of Technology, Tianjin 300401, P. R. China*

Received 25 July 2024, received in revised form 13 October 2024, accepted 25 October 2024

Abstract

Hot-rolled 3207 duplex stainless steel (DSS) was solution treated at 1250 °C for 30 min, and cold rolled at 40–80 % reduction. The superplastic deformation was drawn with a constant speed of 1.5×10^{-3} s^{-1} at 950 °C. The effect of cold-rolling reduction on microstructure and properties of 3207 duplex stainless steel was studied. The results show that austenite and ferrite are elongated along a rolling direction with increased reduction With the increase of reduction, the elongation of 3207 DSS at a high-temperature tensile process increased significantly. When the reduction reached 70 %, the elongation could exceed 100 %. When the reduction rate of cold rolling reached 80 %, the elongation reached the maximum value of 408.63 %. When the reduction was less than 60 %, the peak stress was stabilized at about 300 MPa. When the reduction reached 60 %, the peak stress decreased gradually with the increase of the reduction, and the lowest value, 140.34 MPa, was obtained when the reduction reached 80 %.

K e y w o r d s: 3207 duplex stainless steel, cold rolling reduction rate, microstructure, high-temperature plasticity

1. Introduction

Duplex stainless steel (DSS) is mainly composed of a certain proportion of ferrite and austenite structure, which combines the excellent oxidation resistance and stress corrosion properties of ferrite and the good plasticity and toughness of austenite [1]. Therefore, duplex stainless steel has been widely applied in seawater desalination units, ship manufacturing, building, and chemical industries [2–8].

Superplasticity is a special property of duplex stainless steel during the deformation process at high temperatures and low speeds [9]. Through the superplastic deformation process, the elongation of duplex stainless steel can be achieved higher than 100 % [10]. Therefore, superplastic forming is an important method for many materials, including duplex stainless steel [11, 12]. Research on the superplastic forming of duplex stainless steel is of scientific significance and application value [13, 14].

Superplastic deformation requires a certain microstructure basis. It is generally believed that fine equiaxed grain structure is conducive to the superplastic deformation process [15–17]. Therefore, we assume that cold-rolled duplex stainless steel sheets with different grain sizes can be obtained by cold rolling with different rolling reduction rates after solution treatment and fine equiaxed grain microstructures can be obtained by dynamic recrystallization at high temperatures.

To achieve this purpose, 3207 duplex stainless steel with high corrosion resistance is taken as raw material, and cold rolling with a reduction rate of 40–80 % is carried out after solution treatment at 1250 °C. The effect of rolling reduction rate on the high-temperature plastic deformation of 3207 duplex stainless steel is studied to obtain 3207 duplex stainless steel sheet with superplastic deformation capability.

*Corresponding author: e-mail address: 176833240@qq.com
**Corresponding author: e-mail address: tjjk_zy@126.com

Table 1. Chemical composition of 3207 duplex stainless steel (wt.%)

Cr	Ni	Mo	Mn	Si	C	S	P	N	Fe
31.05	6.64	3.88	1.03	0.15	0.029	0.005	0.014	0.53	Bal.

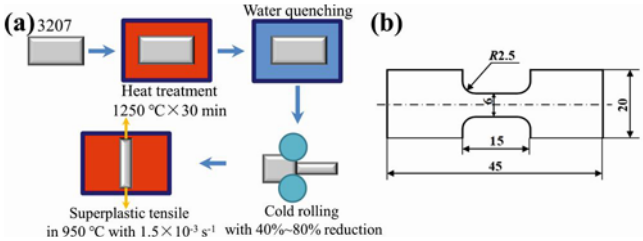

Fig. 1. (a) Schematic illustration of the preparation process of duplex stainless steel and (b) dimensions of a thermostatic tensile specimen.

2. Experiment

2.1. Experimental materials

In this paper, the commercial hot-rolled 3207 duplex stainless steel (produced by Yanbang New Material Technology Co., Ltd., Beijing) is utilized as raw material, and its chemical composition is shown in Table 1. 3207 sheets were cut into sheet specimens with thickness of 3.3, 4.0, 5.0, 6.7, and 10.0 mm by wire-electrode cutting. The length of the specimen was 15 mm, and the width was 5 mm.

2.2. Preparation of duplex stainless steel

Figure 1a shows the preparation process of 3207 duplex stainless steel sheet. First, the wire-cut and cleaned duplex stainless steel specimen was placed in a heating furnace at 1250 ℃ and held for 30 min. When finished, the specimen was quickly removed from the heating furnace and quickly put into cold water for stirring so that its temperature could quickly drop to room temperature. The specimens of different thicknesses were then cold-rolled in multiple passes on a 4-high reversing cold rolling mill so that the final thickness of all specimens should be 2 mm. The actual reduction of each pass in the rolling process was about 0.5 mm, and the final total reduction rate was 40, 50, 60, 70, and 80.

The cold-rolled specimens with different reduction rates were cut by wire-electrode cutting into the geometry shape of the tensile specimen, as shown in Fig. 1b. In the tensile testing machine equipped with a heating furnace, the duplex stainless steel specimen was drawn at constant temperature and constant speed, the temperature for the tensile process was controlled of 950 ℃, and the initial strain rate was $1.5 \times 10^{-3}\,s^{-1}$. The test was repeated three times for each tensile specimen to ensure accuracy, and the average elongation values were calculated. Before drawing, the specimen was assembled on the drawing die and kept in a constant temperature device for 5 min. After a tensile fracture, the specimen was quickly removed and placed into cold water so that its temperature could quickly drop to room temperature.

2.3. Characterization of experimental results

The microstructure of duplex stainless steel after solution treatment and cold rolling with different reduction rates was observed by Imager.M2m metallographic microscope. The phase analysis was performed using a Rigaku X-ray diffractometer, and then the phase composition and grain size were calculated using the XRD pattern. The hardness of duplex stainless steel after solution treatment and cold rolling was measured by a 430SVD micro-Vickers hardness tester. The load size was 9.8 N, and the loading time was 15 s. The thermostatic tensile equipment automatically measured the load and displacement in the thermostatic tensile process, and the true stress-strain curve was drawn from the load-displacement relationship, and the peak stress σ_{max} and the stress $\sigma_{0.1}$–$\sigma_{0.5}$ when the true strain was 0.1–0.5 were calculated. The elongation of the specimen at break was obtained by measuring the actual length of the specimen after breaking/fracturing.

3. Experimental results and discussion

3.1. Microstructure of solution-treated 3207 duplex stainless steel

Figure 2a shows the metallographic structure of 3207 duplex stainless steel after solution treatment at 1250 ℃ for 30 min. It can be observed that after solution treatment, the duplex stainless steel had all formed an equiaxed grain structure, the dark black ferrite and bright white austenite [10, 18] were distributed alternately, and the structure was evenly distributed in three-dimensional space. Figure 2b shows the X-ray diffraction pattern of 3207 duplex stainless steel after solution treatment. It can be observed that the duplex stainless steel after solution treatment consisted of two phases of ferrite (δ) and austenite (γ), and did not contain the precipitated σ phase.

According to the X-ray diffraction pattern shown in Fig. 2b, the value of (111) γ, (200) γ, (220) γ, (311) γ and (110) δ, (200) δ and (211) δ peaks were taken, and the grain sizes of ferrite and austenite phases were calculated according to the Scherrer formula shown in

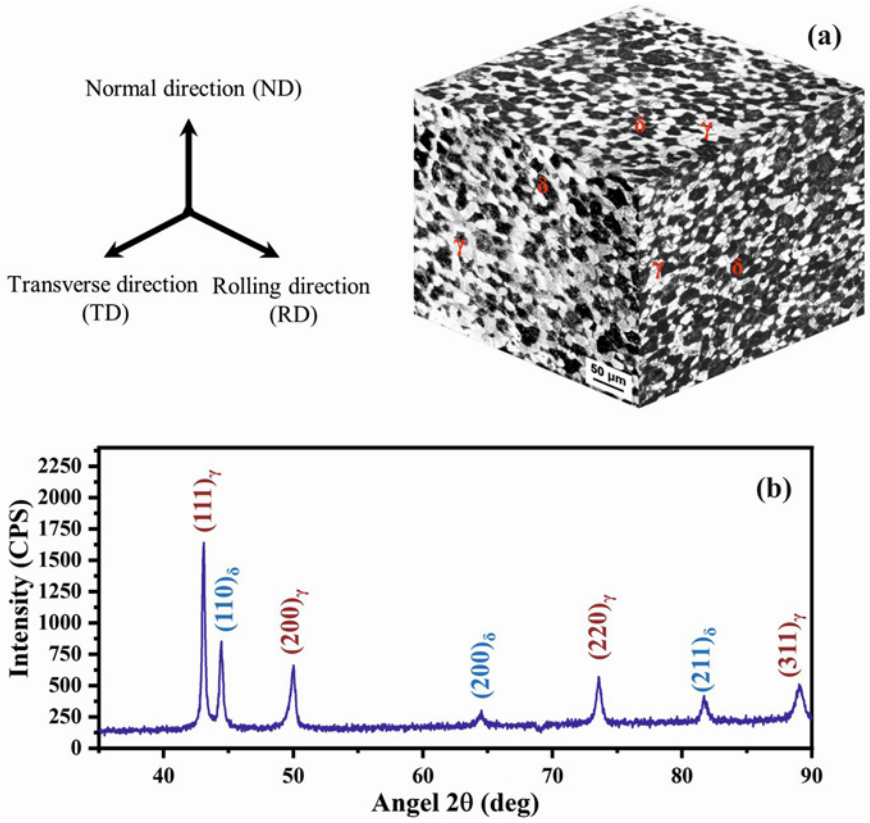

Fig. 2. Structure of solution treated 3207 duplex stainless steel: (a) metallographic structure and (b) X-ray diffraction pattern.

T a b l e 2. Grain size and phase fraction of solution treated 3207 duplex stainless steel

Grain size (nm)		Phase fraction (%)	
Austenite (γ)	Ferrite (δ)	Austenite (γ)	Ferrite (δ)
26.8 ± 8.3	26.7 ± 5.5	77.3	22.7

Eq. (1) [19]:

$$D = \frac{0.9\lambda}{\beta \cos\theta}, \tag{1}$$

where D is the crystal size, λ is the wavelength of $K\alpha$ radiation, β is the full width at half maximum (FWHM), and 2θ is the radiation angle.

The Miller approach (Eq. (2)) is utilized to calculate the phase ratio of ferrite and austenite [20]:

$$V_\gamma = 1.4I_\gamma / \left(I_\delta + 1.4I_\gamma\right), \tag{2}$$

where V_γ is the volume fraction of austenite, I_γ is the comprehensive peak intensity of each diffraction peak of austenite, and I_δ is the comprehensive strength of each diffraction peak of ferrite.

Table 2 shows the grain size (calculated value) and phase composition of the ferrite and austenite structures calculated from the X-ray diffraction pattern in Fig. 3b. It can be seen from the table that the grain size of ferrite and austenite is similar, but the austenite content in the duplex stainless steel after solution treatment is much higher than that of ferrite.

3.2. Microstructure of cold-rolled 3207 duplex stainless steel

Figure 3 shows the microstructure of 3207 duplex stainless steel after cold rolling with a 40–80 % reduction rate, and the yellow line segment in the figure has the same length. As can be seen from the figure, after cold rolling, the duplex stainless steel is still composed of ferrite and austenite in two phases, but both phases are elongated along the rolling direction, evolving from the equiaxed grains after solution treatment into the cold-deformed laminate structure [21, 22]. The laminate spacing between ferrite and austenite decreases with the cold rolling reduction rate increase, but no obvious grain breakage occurs.

The hardness of 3207 duplex stainless steel after solution treatment and cold rolling with 40–80 % reduction rate is presented in Fig. 4. It can be observed

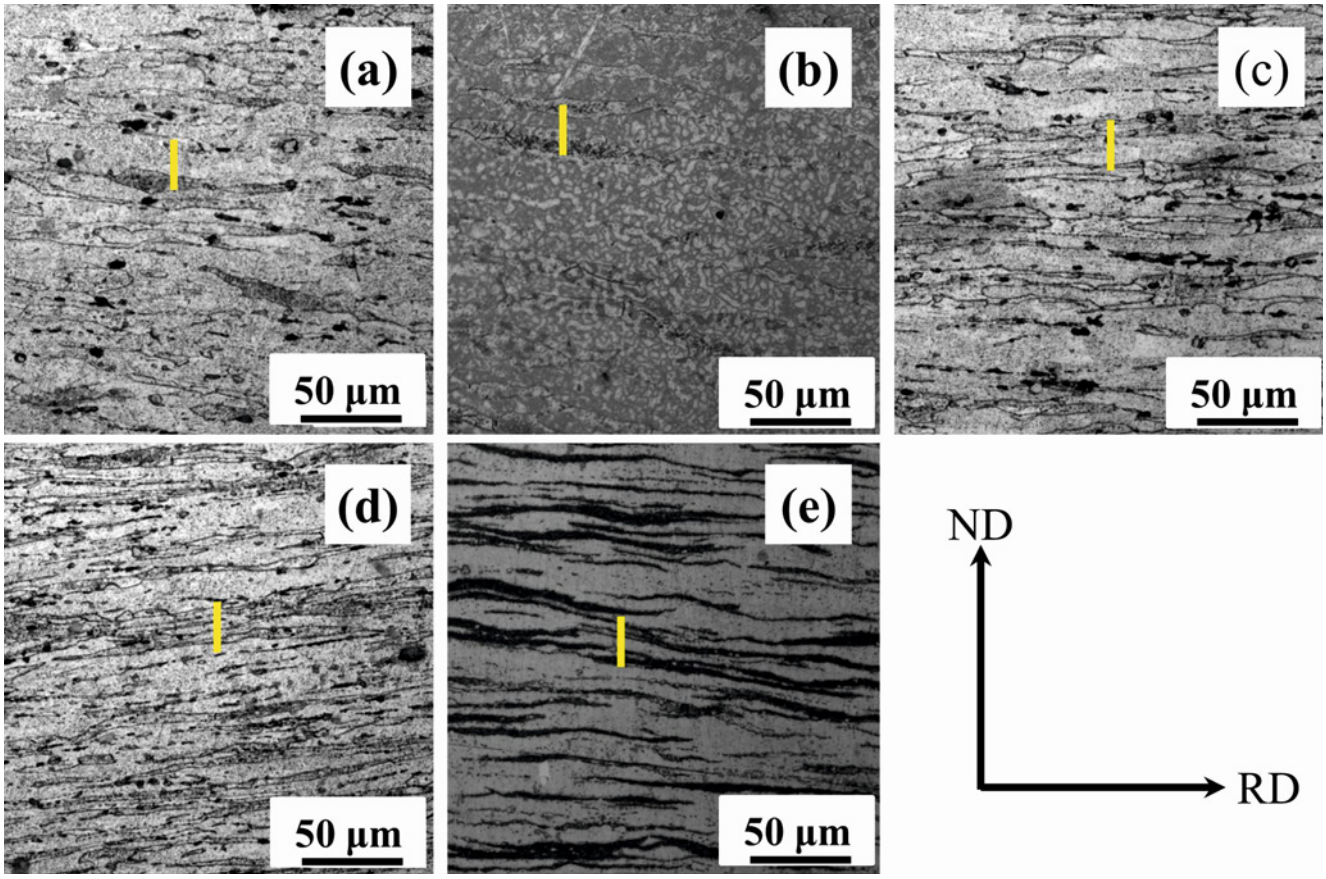

Fig. 3. Metallographic structure of cold-rolled 3207 duplex stainless steel rolling reduction rate: (a) 40 %, (b) 50 %, (c) 60 %, (d) 70 %, and (e) 80 %.

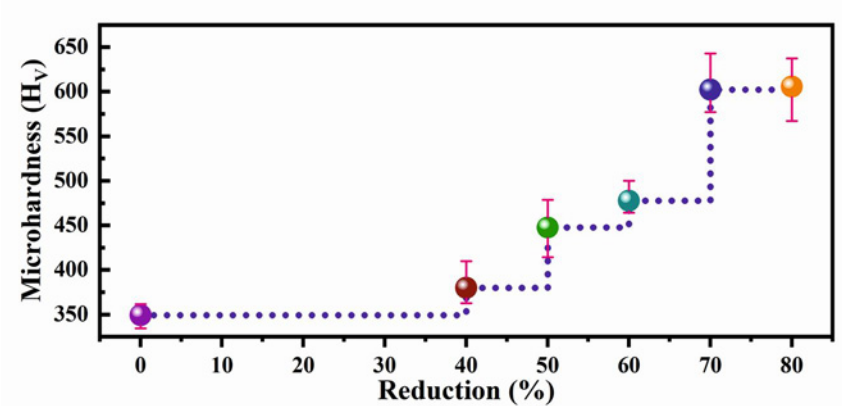

Fig. 4. Effect of cold rolling reduction rate on hardness of 3207 duplex stainless steel.

from the figure that when the rolling reduction rate is lower than 60 %, the hardness of 3207 duplex stainless steel increases slowly with the increase of rolling reduction rate. The hardness of duplex stainless steel increases greatly when the cold rolling reduction rate increases from 60 to 70 %. When the rolling reduction rate increases from 70 to 80 %, the hardness of duplex stainless steel changes gradually.

3.3. High-temperature plastic deformation of 3207 duplex stainless steel

Figure 5a shows the fracture morphology of 3207 duplex stainless steel specimens after solution treatment (recorded as 0 % reduction rate) and cold rolling with different reduction rates. It can be seen from the figure that when the rolling reduction rate is lower than 60 %, the plastic deformation of the specimen is

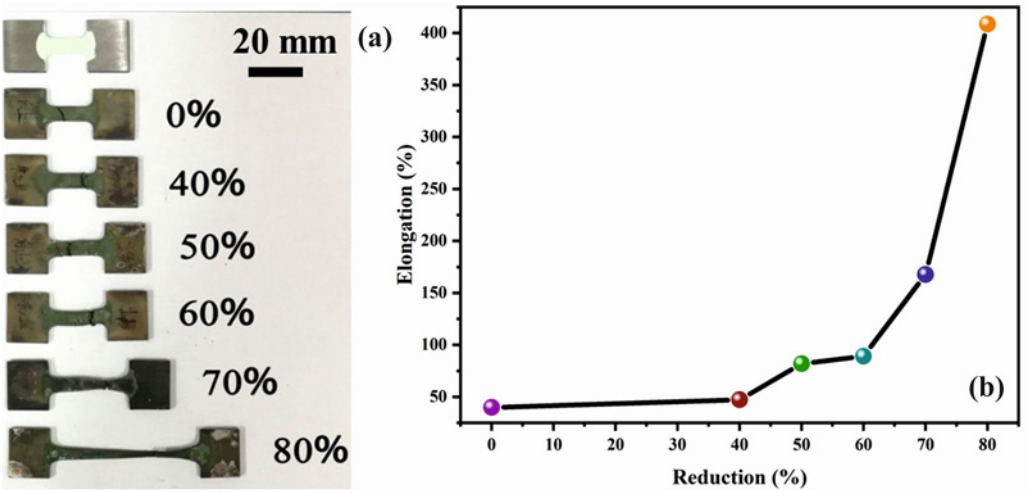

Fig. 5. Photograph of the tensile specimens after tensile testing at high temperature and elongation at break: (a) photograph of the tensile specimens and (b) elongation at break.

small, and the macro fracture is a typical morphology of brittle fracture. When the rolling reduction rate is 70 and 80 %, the specimen has a high elongation at break, and the specimen also has a large plastic deformation during the tensile testing process, resulting in neck shrinkage and, eventually, fracture.

Figure 5b shows the tensile elongation at the break of the specimen. It can be seen from the figure that the elongation at the break of duplex stainless steel increased significantly with the increase of rolling reduction. When the rolling reduction rate is less than 60 %, the elongation at break of duplex stainless steel is below 100 %, and the elongation at break increases slightly with the increase of rolling reduction. When the rolling reduction rate reaches more than 70 %, the elongation at break increases greatly with the increase of the rolling reduction rate. When the rolling reduction rate reaches 80 %, the elongation at the break of duplex stainless steel reaches 408.63 %.

Figure 6a shows the true stress-strain curve of 3207 duplex stainless steel for a high-temperature tensile process. It can be seen from the figure that the true stress-strain curve profile of 3207 duplex stainless steel after solution treatment and cold rolling with a reduction rate of 40–80 % shows that the stress decreases at a certain rate after reaching the peak stress and then decreases abruptly. With the increase in rolling reduction rate, on the one hand, the peak stress in the tensile process changed. On the other hand, the process duration of stress decreases at a certain rate, so the elongation at break is also different. Figure 6b calculates the changes of peak stress and $\sigma_{0.1}$–$\sigma_{0.5}$ in Fig. 6a with the rolling reduction rate. As can be seen from the figure, when the total rolling reduction rate is below 50 %, the peak stress of the duplex stainless steel during the tensile process is higher and stabilized at about 300 MPa. When the rolling reduction rate is above 50 %, the peak stress decreases with

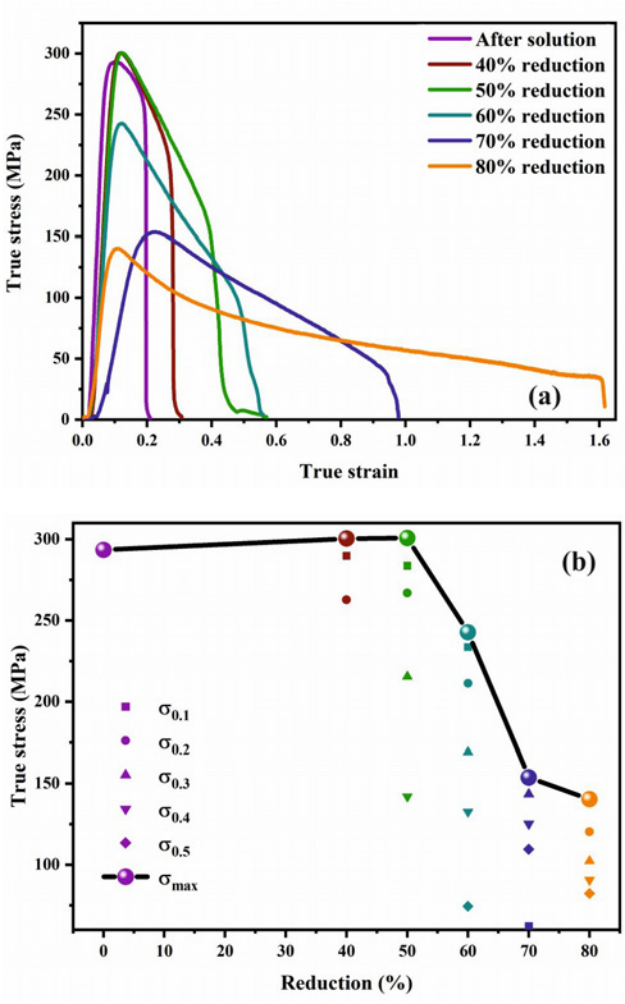

Fig. 6. True stress-strain curve and change of peak and true stress during high-temperature tensile process: (a) true stress-strain curve for high-temperature tensile process and (b) effect of reduction rate on the peak and true stress.

the increase of the rolling reduction rate. When the rolling reduction rate is 80 %, the peak stress is only 140.34 MPa. According to the difference between the peak stress and $\sigma_{0.1}$–$\sigma_{0.5}$ in Fig. 6b, the 3207 duplex stainless sheets of steel cold-rolled with different reduction rates all reach the peak stress at a small strain (0.1–0.2) and then the stress decreases with the increase of the strain. With the increasing rolling reduction rate, the magnitude of stress reduction decreased gradually.

3.4. Mechanism of the effect of cold rolling reduction rate on high-temperature plasticity of 3207 duplex stainless steel

Many studies have shown that cold processing does not affect the phase composition of the material but only changes its structure [23–25]. Therefore, with the increase of rolling reduction rate, the internal phase composition of duplex stainless steel does not change significantly, but the grain refinement shown in Fig. 3 occurs. On the other hand, the relationship between grain size and hardness can be expressed by the Hall-Petch formula shown in Eq. (3) [26]:

$$H = H_0 + Kd^{-\frac{1}{2}}, \tag{3}$$

where H is the theoretical hardness of the material, H_0 and K are functions of material properties, and d is the average grain size. It can be seen from the formula that the hardness of the material is inversely proportional to the square root of the average grain size; that is, the hardness of the material increases with the decrease of the grain size. It can also be seen from the trend of hardness change with the increase of cold rolling reduction rate shown in Fig. 4 that the grain size of 3207 duplex stainless steel decreases with the increase of rolling reduction rate, and the grain refinement is more obvious when the rolling reduction rate is higher than 60 %. The energy applied in the cold rolling process mainly increases the distortional strain energy of duplex stainless steel because the grain breakage effect is insignificant. The energy applied in the cold rolling process mainly increases the distortional strain energy of duplex stainless steel because the grain breakage is not significant. In the process of thermal deformation, high distortional strain energy is more likely to result in dynamic recovery and recrystallization [27], which facilitates the occurrence and continuous progress of superplastic deformation.

4. Conclusions

(1) After solution treatment of 30 min at 1250 °C, austenite and ferrite of 3207 duplex stainless steel are distributed in equiaxed grains alternate phases with similar grain sizes, and the content of austenite is much higher than that of ferrite. With the cold rolling reduction rate increase, austenite and ferrite gradually elongate along the rolling direction. The hardness of 3207 duplex stainless steel increases with the cold rolling reduction rate, and the hardness increases the most when the cold rolling reduction rate is increased from 60 to 70 %.

(2) With the increase of the reduction rate of cold rolling, the elongation at break of 3207 duplex stainless steel at high-temperature tensile process increases significantly, and when the reduction rate of cold rolling reaches 70 %, the elongation at break exceeds 100 %; when the reduction rate of cold rolling reaches 80 %, the elongation at break reaches the maximum, which is 408.63 %.

(3) When the reduction rate of cold rolling is less than 60 %, the peak stress of the tensile process is stabilized at about 300 MPa. When the reduction rate of cold rolling is more than 60 %, the peak stress decreases gradually with the increase of the reduction rate. When the reduction rate of cold rolling reaches 80 %, the peak stress reaches the lowest value, 140.34 MPa. The 3207 duplex stainless steel cold-rolled with different reduction rates reaches the peak stress under small strain, and then the stress gradually decreases with the increase of strain. With the increasing rolling reduction rate, the magnitude of stress reduction decreases gradually.

Acknowledgements

The paper was financially supported by the Natural Science Foundation of Hebei Province (No. E2023202242) and the Chunhui Project Foundation of the Education Department of China (No. HZKY20220264).

References

[1] S. Fashu, V. Trabadelo, A critical review on development, performance and selection of stainless steels and nickel alloys for the wet phosphoric acid process, Mater. Des. 227 (2023) 111739. https://doi.org/10.1016/j.matdes.2023.111739

[2] Y. Sun, X. Tan, R. Lan, G. Ran, J. Li, Y. Jiang, Mechanisms of inclusion-induced pitting of stainless steels: A review, J. Mater. Sci. Technol. 168 (2024) 143–156. https://doi.org/10.1016/j.jmst.2023.06.008

[3] Z. Xu, Y. Hou, M. Nele, G. Li, S. Zhou, High-throughput first-principles study on the effect of Ni segregation on the formation of Cr-depleted zone and corrosion resistance of S32205 duplex stainless steels, J. Mater. Res. Technol. 30 (2024) 3474–3484. https://doi.org/10.1016/j.jmrt.2024.04.082

[4] S. P. Tsai, M. T. Hong, W. H. Lin, S. Y. Lu, Y. R. Jiang, T. W. Lin, P. Y. Tung, Investigation of high-temperature deformation behaviours of a low-carbon

containing duplex stainless steel, J. Mater. Res. Technol. 30 (2024) 7644–7654. https://doi.org/10.1016/j.jmrt.2024.05.098
[5] X. Zhang, J. Li, Q. Gong, C. Liu, J. Li, Deformation behaviors at cryogenic temperature of lean duplex stainless steel with heterogeneous structure prepared by a short process, J. Mater. Res. Technol. 24 (2023) 9273–9291. https://doi.org/10.1016/j.jmrt.2023.05.093
[6] Y. W. Wu, H. Cheng, H. B. Bai, S. Z. Li, Y. Tang, Experimental investigation on static and dynamic energy dissipation characteristics of composite sandwich structure with entangled metallic wire materials and disc springs, Mater. Res. Express. 8 (2021) 106507. https://doi.org/10.1088/2053-1591/ac2b5a
[7] C. G. Bao, C. Zhang, Preparation and corrosion resistance properties of duplex stainless steel (00Cr22Ni6-MnMoCu), Mater. Res. Express. 8 (2021) 126501. https://doi.org/10.1088/2053-1591/ac3bf8
[8] G. N. Ahmad, N. K. Singh, B. N. Tripathi, S. S. A. Askari, S. Pandey, A. Zare, S. M. M. Hasnain, Monitoring of thermo-cycles in fibre laser welding of duplex stainless steel 2205 sheets and its correlation with microstructures and mechanical properties, Mater. Res. Express. 10 (2023) 106517. https://doi.org/10.1088/2053-1591/ad0095
[9] F. Qiang, S. Xin, X. Tu, H. Wang, P. Guo, H. Hou, Z. Lian, L. Zhang, W. Hou, Low-temperature superplastic deformation mechanism of ultra-fine grain Ti-6Al-4V alloy by friction stir processing, J. Mater. Res. Technol. 30 (2024) 7413–7419. https://doi.org/10.1016/j.jmrt.2024.05.150
[10] Q. Zhang, Q. Lian, C. Zhang, F. Peng, J. Han, H. Feng, H. Li, J. Qi, J. Yang, F. Kong, Y. Chen, Superplastic deformation behavior of 5 vol.% (TiB_w+TiC_p)/Ti matrix composite sheets with lamellar microstructure, J. Mater. Res. Technol. 30 (2024) 440–450. https://doi.org/10.1016/j.jmrt.2024.03.074
[11] Y. J. Hu, Y. P. Sun, J. M. He, D. J. Fang, J. X. Zhu, X. C. Meng, Effect of friction stir processing parameters on the microstructure and properties of ZK60 magnesium alloy, Mater. Res. Express. 9 (2022) 016508. https://doi.org/10.1088/2053-1591/ac475e
[12] J. M. He, Y. J. Hu, Y. P. Sun, W. Z. Li, G. J. Luo, Effect of single-pass friction stir processing parameters on the microstructure and properties of 2 mm thick AA2524, Mater. Res. Express. 9 (2022) 096509. https://doi.org/10.1088/2053-1591/ac8f20
[13] X. L. Yang, X. F. Du, Z. L. Xu, Z. S. Liang, L. L. Xiong, Progress in processing of porous titanium: A review, Rare Metal. 43 (2024) 1932–1955. https://doi.org/10.1007/s12598-023-02570-z
[14] Q. Y. Che, K. S. Wang, W. Wang, L. Y. Huang, T. Q. Li, X. P. Xi, P. Peng, K. Qiao, Microstructure and mechanical properties of magnesium-lithium alloy prepared by friction stir processing, Rare Metal. 40 (2021) 2552–2559. https://doi.org/10.1007/s12598-019-01217-2
[15] L. P. Troeger, E. A. Starke Jr., Microstructural and mechanical characterization of a superplastic 6xxx aluminum alloy, Mater. Sci. Eng. A 277 (2000) 102–113. https://doi.org/10.1016/S0921-5093(99)00543-2
[16] F. Musin, R. Kaibyshev, Y. Motohashi, G. Itoh, Superplastic behavior and microstructure evolution in a commercial Al-Mg-Sc alloy subjected to intense plastic straining, Metall. Mater. Trans. A 35 (2004) 2383–2392. https://doi.org/10.1007/s11661-006-0218-4
[17] X. Xu, T. Nishimura, N. Hirosaki, R. J. Xie, Y. Yamamoto, H. Tanaka, Superplastic deformation of nano-sized silicon nitride ceramics, Acta Mater. 54 (2006) 255–262. https://doi.org/10.1016/j.actamat.2005.09.005
[18] Y. Yang, B. Yan, J. Yin, Y. Wang, G. Dong, Microstructure and corrosion behaviour aging at 750 ℃ in 25%Cr duplex stainless steel, Rare Met. 30 (2011) 515–519. https://doi.org/10.1007/s12598-011-0336-z
[19] W. J. Wang, K. C. Yung, H. S. Choy, T. Y. Xiao, Z. X. Cai, Effects of laser polishing on surface microstructure and corrosion resistance of additive manufactured CoCr alloys, Appl. Surf. Sci. 443 (2018) 167–175. https://doi.org/10.1016/j.apsusc.2018.02.246
[20] L. Zhang, R. Song, C. Zhao, F. Q. Yang, Y. Xu, S. G. Peng, Evolution of the microstructure and mechanical properties of an austenite-ferrite Fe-Mn-Al-C steel, Mater. Sci. Eng. A 643 (2015) 183–193. https://doi.org/10.1016/j.msea.2015.07.043
[21] J. Li, X. Ren, Y. Zhang, H. Hou, X. Gao, Effect of superplastic deformation on precipitation behavior of sigma phase in 3207 duplex stainless steel, Prog. Nat. Sci.: Mater. Int. 31 (2021) 334–340. https://doi.org/10.1016/j.pnsc.2020.12.011
[22] J. Li, X. Ren, X. Gao, Effect of superplastic deformation on microstructure evolution of 3207 duplex stainless steel, Mater. Charact. 164 (2020) 110320. https://doi.org/10.1016/j.matchar.2020.110320
[23] S. Tagashira, K. Sakai, T. Furuhara, T. Maki, Deformation microstructure and tensile strength of cold rolled pearlitic steel sheets, ISIJ Int. 40 (2000) 1149–1156. https://doi.org/10.2355/isijinternational.40.1149
[24] L. L. Chang, E. F. Shang, Y. N. Wang, X. Zhao, M. Qi, Texture and microstructure evolution in cold rolled AZ31 magnesium alloy, Mater. Charact. 60 (2009) 487–491. https://doi.org/10.1016/j.matchar.2008.12.003
[25] L. Wang, W. Lu, J. Qin, F. Zhang, D. Zhang, Microstructure and mechanical properties of cold-rolled TiNbTaZr biomedical β titanium alloy, Mater. Sci. Eng. A 490 (2008) 421–426. https://doi.org/10.1016/j.msea.2008.03.003
[26] H. Yu, C. Li, Y. Xin, A. Chapuis, X. Huang, Q. Liu, The mechanism for the high dependence of the Hall-Petch slope for twinning/slip on texture in Mg alloys, Acta Mater. 128 (2017) 313–326. https://doi.org/10.1016/j.actamat.2017.02.044
[27] F. Q. Yang, R. B Song, L. F. Zhang, C. Zhao, Hot deformation behavior of Fe-Mn-Al light-weight steel, Procedia Eng. 81 (2014) 456–461. https://doi.org/10.1016/j.proeng.2014.10.022